nature communications

Article

https://doi.org/10.1038/s41467-024-51921-6

Regulatory transposable elements in the encyclopedia of DNA elements

Received: 7 October 2023

Accepted: 16 August 2024

Published online: 31 August 2024

Check for updates

Alan Y. Du[1,2,5], Jason D. Chobirko[3,5], Xiaoyu Zhuo[1,2,5], Cédric Feschotte[3] & Ting Wang[1,2,4]

Transposable elements (TEs) comprise ~50% of our genome, but knowledge of how TEs affect genome evolution remains incomplete. Leveraging ENCODE4 data, we provide the most comprehensive study to date of TE contributions to the regulatory genome. We find 236,181 (~25%) human candidate cis-regulatory elements (cCREs) are TE-derived, with over 90% lineage-specific since the human-mouse split, accounting for 8–36% of lineage-specific cCREs. Except for SINEs, cCRE-associated transcription factor (TF) motifs in TEs are derived from ancestral TE sequence more than expected by chance. We show that TEs may adopt similar regulatory activities of elements near their integration site. Since human-mouse divergence, TEs have contributed 3–56% of TF binding site turnover events across 30 examined TFs. Finally, TE-derived cCREs are similar to non-TE cCREs in terms of MPRA activity and GWAS variant enrichment. Overall, our results substantiate the notion that TEs have played an important role in shaping the human regulatory genome.

Barbara McClintock, who discovered TEs in maize[1], was the first to recognize their ability to act as *cis*-regulatory elements (CREs) controlling the expression of nearby genes. In the ensuing decades, it became clear that a large fraction of the genome of multicellular organisms consists of interspersed repeats primarily derived from TEs. In mammals, TEs account for 28–75% of the genome sequence[2]. In humans, at least 46% of the ~3.1 GB haploid genome is derived from TEs[3]. Most TEs in the human genome can be classified into LINE, SINE, LTR and DNA transposon classes. LINEs are autonomous retrotransposons that use target primed reverse transcription to insert into the genome. SINEs are short, non-autonomous elements that rely on the LINE machinery to mobilize. LTR elements in the human genome are mostly derived from endogenous retroviruses (ERVs) which expand using the retroviral replication mechanism. Unlike the other three classes which use RNA intermediates to transpose, DNA transposons mobilize directly via a “cut-and-paste” DNA mechanism[4]. The vast majority of human TEs have long ceased transposition activity, and only a small subset of LINEs and SINEs are known to be currently capable of mobilization in modern humans.

Although McClintock viewed TEs as essential “controlling elements”, it is clear that the vast majority of TE sequences in the human genome have not evolved under functional constraint and therefore do not appear to contribute significantly to organismal fitness[5]. Still, about 11% of evolutionarily constrained bases in human fall under TEs[5], and there have been many reports showing that some TEs function as CREs, including promoters and enhancers, regulating important biological processes (reviewed in refs. 6–11). However, we still lack a global picture of how many CREs are derived from TEs and how many are truly functional.

Another fundamental question concerns the evolution of TEs from selfish elements to CREs co-opted for gene regulation. One model postulates that TEs ancestrally harbor CREs and transcription factor binding sites (TFBSs) in order to regulate their own genes, which are then occasionally co-opted for regulating host gene expression. Many examples of previously characterized TE-derived CREs are consistent with this ancestral origin model[12–15]. An alternative model is that TEs acquire TFBSs and *cis*-regulatory activity post-insertion through mutation over time. This has been observed for P53, PAX-6, and MYC

[1]Department of Genetics, Washington University School of Medicine, St. Louis, MO, USA. [2]The Edison Family Center for Genome Sciences and Systems Biology, Washington University School of Medicine, St. Louis, MO, USA. [3]Department of Molecular Biology and Genetics, Cornell University, Ithaca, NY, USA. [4]McDonnell Genome Institute, Washington University School of Medicine, St. Louis, MO, USA. [5]These authors contributed equally: Alan Y. Du, Jason D. Chobirko, Xiaoyu Zhuo. e-mail: cf458@cornell.edu; twang@wustl.edu

TFBSs in human Alu SINE elements and circadian clock TFBSs in mouse RSINE1 elements, in which imperfect binding motifs matured into canonical binding motifs over evolutionary time[16–18].

The ENCODE and Roadmap projects have sought to characterize the landscape of CREs in the human genome, providing invaluable resources for scientists all over the world[19,20]. Data from these projects have facilitated systematic investigation of TE contributions to regulatory functions in the genome[21,22]. In ENCODE phase 3, genome-wide annotations of candidate *cis*-regulatory elements (cCREs) were created in both human and mouse genomes[19]. Based on four epigenomic assays and gene annotation, cCREs were classified into promoter-like sequence (PLS), proximal enhancer-like sequence (pELS), distal enhancer-like sequence (dELS), high-H3K4me3 elements (DNase-H3K4me3), and potential boundary elements (CTCF-only). Regions with enhancer signal were separated into pELS and dELS based on their distance to annotated transcription state sites (TSSs). DNase-H3K4me3 cCREs represent regions with promoter signal without a nearby annotated TSS. CTCF-only cCREs represent regions that could be genome folding anchors or other architectural elements. Altogether, cCREs comprise 7.9% and 3.4% of human and mouse genomes, respectively. In the latest ENCODE phase 4, functional assays such as massively parallel reporter assay (MPRA) have been included to validate regulatory element predictions. Here we leverage these resources to quantify the contribution of TEs to the regulatory genome and derive general principles for how TEs become regulatory elements.

Results

Landscape of TE-derived cCREs in human

To broadly characterize the contribution of TEs to the human regulatory genome, we intersected TEs with cCREs from the version 2 registry of cCREs[19]. As a conservative estimate, we considered cCREs with at least 50% of their sequences coming from a single annotated TE to be TE-derived. Using this criterion, we found that TEs supply ~25% (236,181/926,535) of all human cCREs (Fig. 1A). When cCREs are separated by annotation type, TE contribution ranges from 4.6% in PLS to 38.2% in CTCF-only cCREs. Compared to their genomic proportion, TEs are generally underrepresented in all types of cCREs (Supplementary Fig. 1). Notably, TEs are most depleted in PLS, possibly due to a combination of purifying selection against TE insertion in promoters and incomplete annotation of TE promoters. By contrast, DNase-H3K4me3 and CTCF-only cCREs were enriched for the LTR class of elements ($\log_2$ enrichments of 0.42 and 0.46, respectively). These results suggest that LTR elements have been a prominent source of non-canonical promoters and CTCF binding sites, an observation consistent with previous reports[23–26].

Within each TE class, TEs are further subdivided into many subfamilies of variable age and sequence composition. Thus, we next examined TE contributions to the human regulatory genome at the subfamily level. In terms of absolute numbers of cCRE-associated TEs, LINE and SINE classes contribute the most cCREs per subfamily on average (~5 times more than LTR and ~9 times more/contributed by a single TE, resultin/ than DNA elements) (Fig. 1B). On the other hand, after normalizing to genomic abundance, the LTR class is the most enriched per subfamily on average for cCREs (~4 times more than LINE/SINE and ~2 times more than DNA elements) (Fig. 1C). These results confirm that LTR elements are generally more likely to supply cCREs in the human genome, possibly because they contain strong promoter and enhancer sequences[10]. However, numerically the majority of TE-derived cCREs come from SINEs and LINEs due to their sheer abundance in the human genome.

Considering that regulatory elements are often active in a cell-type-specific manner, we evaluated the contribution of TEs to each of the 25 ENCODE cell/tissue types with full cCRE profiling. Overall, TEs make up between 9 and 19% of cCREs across cell/tissue types (Fig. 1D). The proportion of TE classes contributing to cCREs stays relatively stable across cell/tissue types (Supplementary Fig. 1). Next, we examined whether TE-derived cCREs are more or less likely to be cell-type specific compared to non-TE cCREs. We grouped all cCREs by the number of cell types that share them. With more ubiquitously active cCREs across the 25 fully profiled cell/tissue types (i.e., less cell-type specific), the percentage of cCREs that are TE-derived decreases (Fig. 1E), indicating that cCREs contributed by TEs are more likely to be cell-type specific. This observation is consistent with previous reports that find TEs to contribute cell-type specific regulatory elements[21,27,28].

Evolution of TE-derived cCREs across human and mouse

Next, we investigated the contribution of TEs in the evolution of cCREs in the human and mouse lineages. Starting from 926,535 human cCREs, we identified syntenic mouse regions using UCSC liftOver[29], yielding 601,136 syntenic regions corresponding to ~66% rate of synteny (Fig. 2A, Supplementary Fig. 2). This is significantly higher than the ~40% rate of synteny based on whole genome comparison ($p = 1.5 \times 10^{-323}$, binomial test), which is expected as cCREs should be enriched for functional regulatory elements and therefore more evolutionarily constrained[30]. To identify cCREs derived from TEs orthologous in human and mouse (acquired from their common ancestor), we required that the human cCRE be TE-associated and the corresponding mouse syntenic region contains the same annotated TE ("Methods"). As expected, orthologous TEs are primarily composed of old TE subfamilies that exist in both human and mouse (Supplementary Fig. 2). This approach identified 18,010 TE-derived human cCREs (1.9% of all human cCREs) with a mouse orthologous sequence. Overall, 97% (228,670/236,181) of human TE-derived cCREs are only found in the human lineage. We performed the reciprocal analysis starting from mouse cCREs and found similar results: 1.7% (5900/339,815) of mouse cCREs are TE-derived and have human orthology, and 93% (38,815/41,800) of mouse TE-derived cCREs are only found in the mouse lineage. Thus, TE-derived cCREs are overwhelmingly lineage-specific, and ancient TEs are a minor source of cCREs shared between human and mouse.

To investigate how often orthologous TEs evolve shared function across lineages, we first searched for orthologous TEs with conserved *cis*-regulatory function in human and mouse. Of 98,278 human cCREs with the same syntenic mouse cCRE, 1575 (1.6%) are derived from orthologous TEs. This is similar to the percentage of human cCREs that are TE-derived and have a mouse TE ortholog (1.9%), indicating that conserved regulatory elements are not enriched for TEs. We next asked whether orthologous TEs and non-TE syntenic sequences have different annotations between human and mouse. We categorized each human-mouse pair of sequences into same cCRE type (same), shared cCREs but different type (different), or lineage-specific cCREs. Regardless of cCRE type, orthologous TEs contributing cCREs in human display a significantly different proportion of same, different, and lineage-specific cCRE annotations compared to non-TE sequences (Fig. 2B). Contrary to the null expectation where the proportions are the same between TEs and non-TEs, orthologous TEs that contribute cCREs are more lineage-specific than the non-TE syntenic background, ranging from 7.9% difference for dELS to 41.2% difference for PLS in human (Exact multinomial tests, $p < 0.001$). We performed the same analyses starting from mouse cCREs and found similar results, with differences ranging from 8.7% for DNase-H3K4me3 to 36% for PLS (Supplementary Fig. 2, exact multinomial tests, $p < 0.001$). This suggests that among cCREs with a shared sequence origin, TEs are more likely to diverge in *cis*-regulatory activity to provide lineage-specific function compared to non-TE sequences.

Sequence conservation is generally a good indicator for conserved function. Since we can be confident that orthologous TEs in human and mouse descend from a common ancestor, we tested whether sequence conservation as measured by phastCons score is correlated with their shared annotation as cCREs. Considering only TE

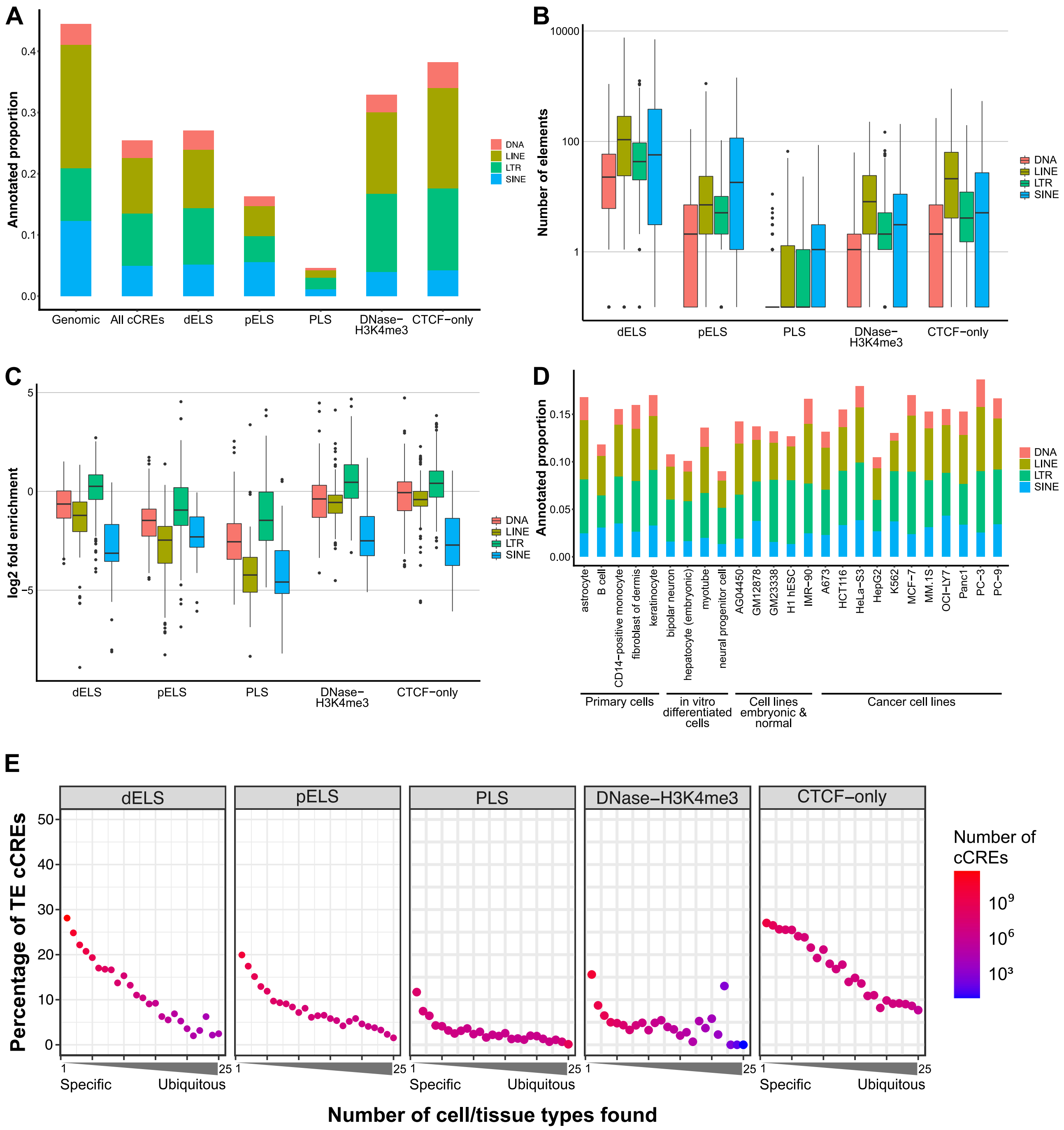

Fig. 1 | Overlap of TEs with human cCREs. A Proportion of genome and cCREs that are TE-derived. **B** Number of elements per TE subfamily, grouped by TE class, that are associated with a cCRE. **C** Enrichment of TE subfamily overlapping with cCREs relative to their abundance in the genome, grouped by TE class. Shown in (**B**) and (**C**) are 326 DNA transposons subfamilies, 184 LINE subfamilies, 595 LTR subfamilies, and 61 SINE subfamilies annotated by RepeatMasker. **D** Proportion of cCREs that are TE-derived across 25 fully profiled cell/tissue types. **E** Percentage of cCREs that are TE-derived for cell/tissue specific cCREs to ubiquitously used cCREs. The x-axis is the number of fully profiled cell/tissue types in which the cCRE is found. cCRE candidate *cis*-regulatory element, dELS distal enhancer-like sequence, pELS proximal enhancer-like sequence, PLS promoter-like sequence, TE transposable element. For all boxplots in this paper, box, interquartile range (IQR); center, median; whiskers, 1.5 × IQR.

subfamilies that are ancestral to human and mouse, we confirmed that orthologous TE sequences have higher phastCons scores than non-orthologous TEs (Wilcoxon test, $p < 2.2 \times 10^{-16}$) (Fig. 2C). Furthermore, we found that orthologous TEs with shared cCRE annotation have higher phastCons scores compared to orthologous TEs with lineage-specific cCRE annotation (Wilcoxon test, $p < 2.2 \times 10^{-16}$) (Fig. 2D). This result suggests that TE-derived cCREs shared by both species are under stronger functional constraint than those that are lineage-specific cCREs. Thus, this set of ~1500 orthologous TE-derived cCREs are strong candidates for being co-opted for important and conserved cellular function.

Given that most human TE-cCREs are not found in mouse and vice versa, we sought to quantify the contribution of TEs to lineage-specific cCREs relative to non-TE sequences. In human, 85% (788,108/926,535) of cCREs were identified as lineage-specific due to either lack of syntenic sequence in mouse or synteny with no mouse cCRE. Among

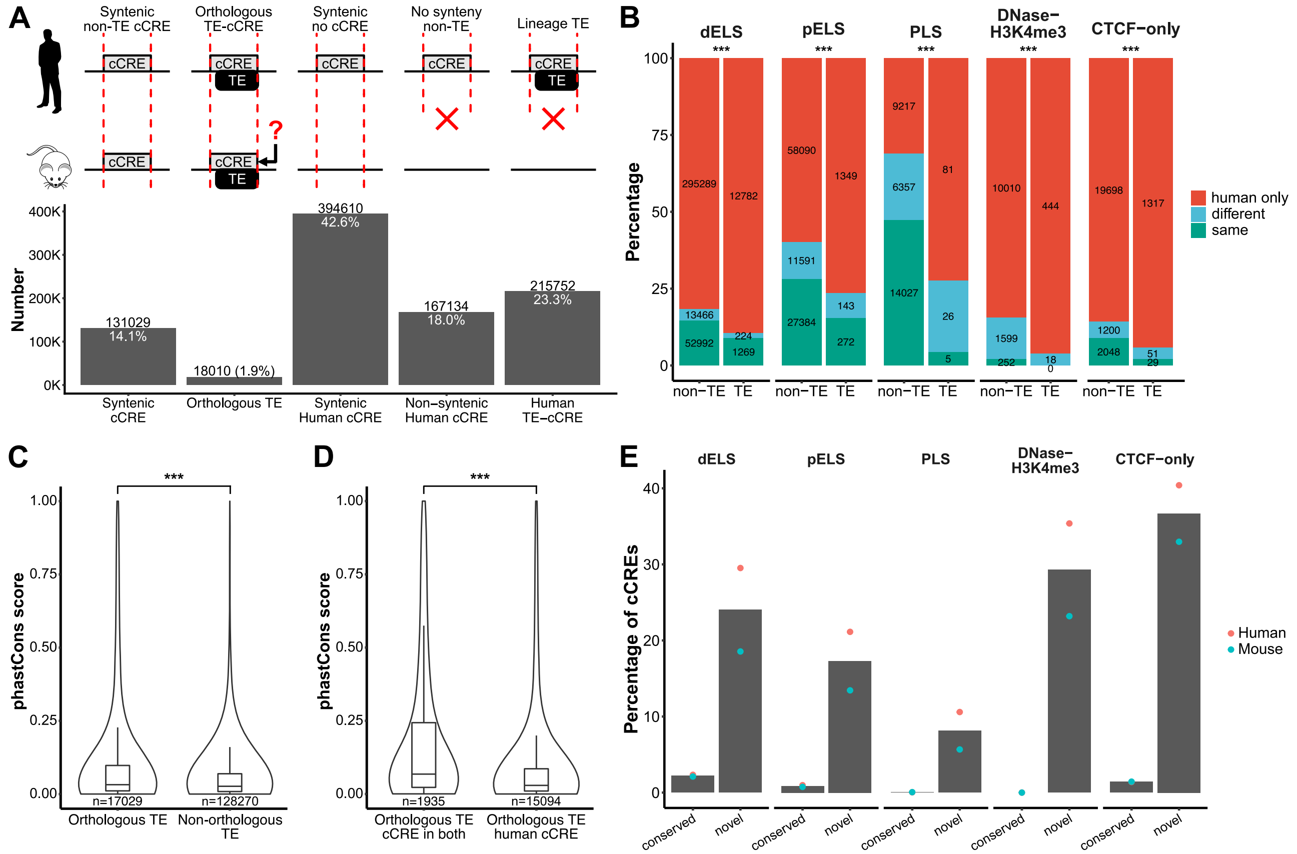

Fig. 2 | TE-derived conserved and lineage-specific cCREs in human and mouse. **A** Classification of shared and lineage-specific cCREs for human to mouse comparison. For orthologous TE-cCREs, syntenic cCRE in mouse is not required but can be present. **B** Percentage of cCREs that are shared or lineage-specific for orthologous TE and syntenic non-TE human anchored cCRE regions. Shared cCREs are split into "same" and "different" categories depending on the syntenic human and mouse cCRE types. Grouping by cCRE type is done using the anchored human cCRE. Multinomial tests for goodness of fit (log-likelihood ratio, exact or Monte Carlo simulations with 1,000,000 random trials) were performed to compare TE and non-TE distributions (dELS Monte Carlo p-value = 0; pELS Monte Carlo p-value = 0; PLS exact p-value = 3.922×10^{-26}; DNase-H3K4me3 exact p-value = 3.975×10^{-16}; CTCF-only exact p-value = 7.233×10^{-28}; no multiple test correction). **C** 100-way vertebrate phastCons score distributions for orthologous TEs and non-orthologous TEs associated with human cCREs. One-sided Wilcoxon rank-sum test p-value < 2.2×10^{-16}. **D** 100-way vertebrate phastCons score distributions for orthologous TEs that have cCRE in both human and mouse vs. human only. One-sided Wilcoxon rank-sum test p-value < 2.2×10^{-16}. **E** Percentage of conserved and novel (lineage-specific) cCREs that are TE-derived, split up by cCRE type. Percentages for human and mouse are shown by red and blue dots, respectively. Bars represent the mean percentage between human and mouse. ***$p < 0.001$.

human lineage cCREs, 29% (228,670/788,108) could be attributed to TEs. In mouse, 61.6% (209,338/339,815) of cCREs were identified as lineage-specific, of which 18.5% (38,815) were TE-associated. We found that TEs have contributed between 6 and 38% of lineage-specific cCREs depending on cCRE type, with the lowest contribution to PLS and the highest to CTCF binding sites (Fig. 2E). Despite more cCRE data being available for human compared to mouse, we observed a similar trend in human and mouse in which TEs supplied 10–40% of human lineage cCREs and 6–33% of mouse lineage cCREs. Overall, these results support the long-standing hypothesis that TEs have had a substantial impact on *cis*-regulatory innovation during mammalian evolution[31–34].

Origin of cCRE-associated transcription factor motifs in TEs

As TFBSs are a major component in driving *cis*-regulatory activity of a sequence, we looked for TF motifs that are associated with cCRE activity in TEs. For each TE subfamily defined by RepeatMasker, we looked for TF motifs that are enriched in cCRE-associated copies of the subfamily relative to non-cCRE copies of the same subfamily (Supplementary Fig. 3A, "Methods"). By using copies of the same TE subfamily as background sequences in this analysis, we minimize the influence of TF motifs that are merely enriched in the TE subfamily compared to the rest of the genome. In total, we could detect 1183 cCRE-associated TF motifs across 376 TE subfamilies (Supplementary Fig. 3B). The TFs most frequently associated with cCREs include AP1, CTCF, ETS, KLF, and Ebox motifs (Supplementary Data 5).

We investigated whether cCRE-enriched TF motifs likely originated from the ancestral TE or arose through mutations after insertion. We first asked what percentage of cCRE-enriched motifs can be identified in the TE's consensus sequence, which represents their ancestral TE sequence. Of 1183 motifs, 541 (46%) are found in consensus sequences (Supplementary Fig. 3C). Notably, SINEs have the lowest percentage (mean of 12%) among TE classes. To increase resolution and specificity, we extended our analysis to consider motif location for individual TE copies. If a TF motif is truly derived from its ancestral TE insertion, we expect the motif to be in the same relative position as the consensus sequence's motif. Thus, we inferred the ancestral origin of each TE's motifs based on the presence or absence of the motif within 10 bp of a consensus motif (Fig. 3A). At a mean of 7%, SINEs once again have the lowest percentage of ancestrally derived TF motifs (percent ancestral origin) for cCRE-associated motifs across TE subfamilies (Fig. 3B). We also observed that cCRE-associated TF motifs have significantly higher percent ancestral origin compared to randomly selected motifs for DNA transposons ($p = 1.2 \times 10^{-8}$), LINEs ($p = 8.7 \times 10^{-8}$), LTRs ($p < 2.2 \times 10^{-16}$), and ERV internal regions (ERV-int) ($p = 0.0067$). This suggests that ancestral TE sequences serve as an important source of TF motifs in cCREs for most but not all TE classes.

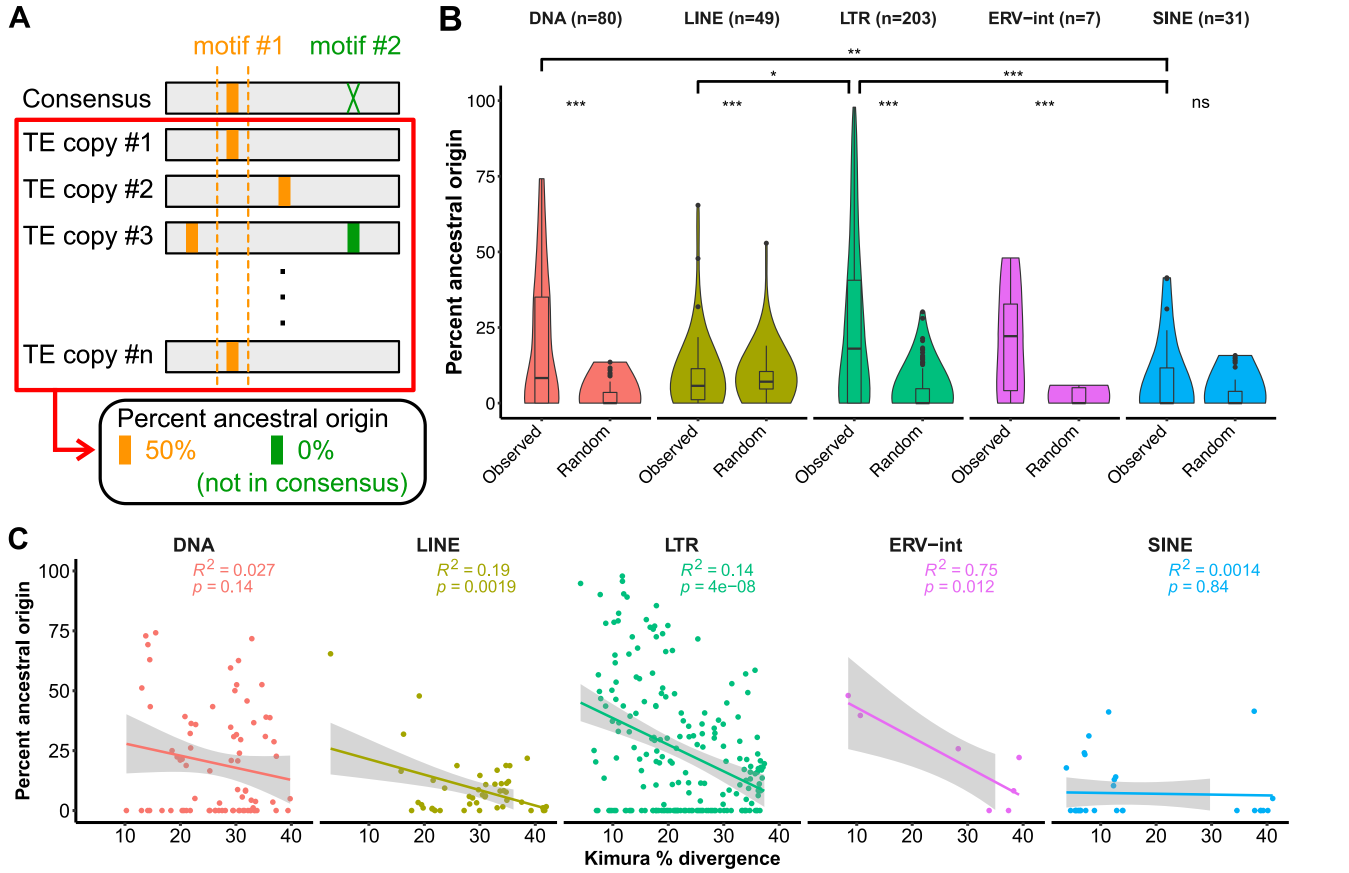

Fig. 3 | cCRE-enriched TF motifs are mostly ancestral except in SINE. **A** Calculation of ancestral origin percentage for cCRE-associated TF motifs. For TF motifs found in the TE subfamily consensus sequence (motif #1), percent ancestral origin was calculated as the percentage of motifs in individual TE copies that align to within 10 bp of the consensus motif (dotted line). For TF motifs that are not found in the consensus sequence (motif #2), we assumed that the TE subfamily's ancestral sequence did not contain the TF motif and all instances of the motif arose through mutation. The mean percentage was taken across all cCRE-associated TF motifs for a TE subfamily to equally weight each TF motif. **B** Distribution of mean percent ancestral origin of cCRE-associated TF motif for each TE subfamily, separated by TE class. Two-sided Wilcoxon rank-sum test with Benjamini–Hochberg correction was performed to compare percent ancestral origin between observed cCRE-associated TF motifs and randomly selected TF motifs (DNA transposons *p*-value = 1.17 × 10^{-8}, LINE *p*-value = 8.71 × 10^{-8}, LTR *p*-value < 1.1 × 10^{-15}, ERV-int *p*-value = 0.00668, SINE *p*-value = 0.863), and to compare percent ancestral origin between TE classes (DNA transposon vs. SINE *p*-value = 0.0097, LTR vs. LINE *p*-value = 0.0239, LTR vs. SINE *p*-value = 0.0002). **C** Correlation between TE subfamily Kimura divergence and cCRE-associated TF motif percent ancestral origin. R-squared and *p*-values for each linear regression is shown along with the 95% confidence interval band. The TE subfamily Kimura divergence represents the age of the TE subfamily given the neutral evolution of most TEs. $^*p < 0.05$, $^{**}p < 0.01$, $^{***}p < 0.001$.

For SINEs, the percentage of cCRE-associated motifs of ancestral origin was not different from random expectation ($p = 0.86$), indicating that the ancestral TE sequence does not generally explain the presence of TF motifs enriched within SINE-derived cCREs.

Next, we considered the evolutionary fate of TF motifs within TE sequences. If TEs contain ancestral TF motifs that are occasionally retained within cCREs, we expect many ancestrally derived TF motifs to gradually decay away through accumulated mutations as most TE copies neutrally evolve. Consistent with this prediction, TE subfamily age, as measured by the mean Kimura divergence of individual copies from the subfamily consensus, is negatively correlated with the percentage of ancestrally derived TF motifs (Fig. 3C). When we break down this analysis per TE class, we found that this correlation held for LINEs, LTRs, and ERV-int, but not for DNA transposons or SINEs. As an orthogonal analysis, we calculated the percentage of TE copies containing the TF motif within each subfamily, based on the hypothesis that ancestrally derived motifs should be found in a higher percentage of copies compared to mutation-derived motifs. TE subfamily age was negatively correlated with the percentage of copies with motif for all TE classes except for SINEs (Supplementary Fig. 3E). Taken together, these findings suggest that most TE subfamilies arrive in the genome already containing *cis*-regulatory sequence features that are retained within cCREs. SINEs tend to adopt a different trajectory whereby TF motifs do not preexist within their ancestral sequence but evolve subsequently via mutations. It is important to note the considerable variation between different TE subfamilies, highlighting that each TE subfamily has its own unique evolutionary path to maintain or acquire *cis*-regulatory activity.

Examining the consensus coverage of cCRE-associated TEs compared to non-cCRE TEs revealed an unexpected enrichment over the 5′ end of LINE1, even after controlling for length (Supplementary Figs. 4 and 5). This indicates that LINE1s that contain the 5′ end disproportionately contribute to cCREs. Our observation is consistent with the prediction that the 5′ region of LINE1 harbors their promoter sequence and contains a wealth of TFBSs[35–38]. These results suggest that the 5′ end of LINEs may be similar to LTRs in providing regulatory sequence.

Genomic context influences the *cis*-regulatory potential of TEs

As TEs are not evenly distributed throughout the genome, we next sought to explore whether there is any relationship between the genomic loci of TE-derived cCREs and non-TE cCREs. Specifically, we quantified the relative distance, or normalized distance between two genomic loci, from either TEs or cCRE-associated TEs to the nearest non-TE-derived cCREs. Here, we zoomed in to focus on relative distance from 0 to 0.1 where the differences were most prominent. If TEs randomly develop into cCREs regardless of their insertion location, we should observe a uniform distribution (a flat line in the relative distance plot) of distances between cCRE-associated TEs and non-TE cCREs. As expected, TE insertions are uniformly distributed in the genome relative to cCREs (left panels in Fig. 4A). However, TEs associated with PLS, pELS, and DNase-H3K4me3 are significantly closer to other cCREs of the same category (higher proportion at low relative distances) when using a cell type-agnostic approach by Kolmogorov–Smirnov test (KS test) (middle panels in Fig. 4A). While not significantly closer when considering cell type-agnostic annotations of dELS, TEs associated with dELS are significantly closer to non-TE dELS sites after separating dELS by cell or tissue type (brown lines in right panels in Fig. 4A). This suggests that, despite being uniformly distributed in the genome in general, TE insertions close to other promoters or enhancers are more likely to be promoters or enhancers themselves. At the TE class level, LTR elements associated with cCREs are more likely to be distant from non-TE cCREs (Fig. 4A), which implies that LTRs are less dependent on genomic context in displaying regulatory activity compared to other TE classes. Lastly, we found that the distances from TEs associated with CTCF-only sites to non-TE CTCF-only sites are more consistent with random distribution in both human and mouse (red lines in Fig. 4A and Supplementary Fig. 6A), despite abundant B2-derived CTCF binding sites in the mouse genome[25]. This indicates that CTCF binding sites provided by TEs are scattered randomly in the genome, which could facilitate formation of new chromatin boundaries. We performed the same analysis using mouse cCREs and TEs and found all trends observed in human to be consistent in the mouse genome (Supplementary Fig. 6A).

To further probe the connection between linear genomic distance and TE-derived *cis*-regulatory activity, we next examined the distance of TEs to TFBSs in K562 cells. For each of 409 TFs with ChIP-seq datasets where at least one TE subfamily was bound at least 10 times, we compared the distance of TF-bound TEs to their nearest non-TE TFBS of the same TF to that of non-bound TEs of the same subfamily. Across all TFs, we found that TF-bound TE copies are ~10 times closer to non-TE TFBSs of the same TF than non-bound TE copies, regardless of TE class (Fig. 4B). These results are consistent with our distance analysis with cCREs and suggest that TEs with *cis*-regulatory activity tend to be proximal to other *cis*-regulatory elements.

Since TF-bound TEs tend to reside near non-TE TFBSs, we hypothesized that TEs can introduce local redundancy in TF binding, which may promote TFBS turnover during evolution[39–42], whereby the TE-derived TFBS can functionally replace the nearby ancestral TFBS. To test this hypothesis, we selected all TFs (30) with high-quality ChIP-seq data in both human K562 and mouse MEL erythroleukemic cells, which are biologically homologous. As reported previously[43], we found that up to ~40% of TFBSs are contributed by TEs in each cell line (Fig. 4C). While most TFBSs in TEs are derived from species-specific TEs, 13–54% and 20–58% of TE-derived TFBSs are syntenic in both human and mouse, respectively. These syntenic TEs are frequently bound by TFs in just one lineage (syntenic but specific). This suggests that TEs are involved in a dynamic evolutionary process where TFBSs can be gained or lost in one lineage through lineage-specific mutations. In addition to providing space for innovation by providing novel TFBSs, TEs are also thought to help maintain local TFBSs through TF turnover. To identify putative TFBS turnover events, we searched for lineage-specific TFBSs within 5 kb of a syntenic TFBS in the other lineage and inferred which TFBS was ancestral based on synteny and phastCons score (Supplementary Fig. 7A). Using this approach, we discovered a total of 6700 and 9245 putative TFBS turnover events across 30 TFs in human and mouse, respectively (Supplementary Fig. 7B). TEs make up 3–56% of putative turnover events, with most derived from lineage-specific TE insertions (Fig. 4D, E). The TFs with the highest TE-derived turnover rates are CTCF and RAD21 in mouse, both of which are part of the cohesin loading complex. These results are consistent with previous studies that have found TEs to participate in CTCF binding site turnover after human-mouse divergence[25]. Our findings point to TEs as important drivers of TFBS turnover during evolution.

TE- and non-TE-derived cCREs have similar features

Since TEs contribute a large proportion of cCREs across the human genome, we explored whether TE-derived cCREs have distinct properties from non-TE cCREs. First, we considered sequence intrinsic *cis*-regulatory activity as measured by MPRA. Using ENCODE phase 4 lentivirus-based MPRA (lentiMPRA) data in K562 cells, which assayed all open chromatin sites in K562, we asked if the tested genomic sequences display differential regulatory activity based on TE annotation[44]. We classified sequences as TE-associated if at least 50% of the sequence is contributed by a single TE, resulting in ~34,000 TE-associated and ~81,000 non-TE sequences tested by MPRA. We further split sequences based on cCRE type. Overall, TE-associated sequences have similar or higher levels of MPRA activity compared to non-TE sequences of the same cCRE type (Fig. 5A). MPRA activity was significantly higher for TE-associated sequences in all cCRE types except PLS and CTCF-bound cCREs (Wilcoxon rank-sum test, pval <0.05), but the differences in activity were subtle (median $\log_2$ fold change difference of 0.207, 0.060, 0.060, 0.078, and 0.052 for DNase-H3K4me3, dELS, pELS, DNase-only, and None, respectively). This is consistent with a previous study that found TE sequences of one LTR subfamily with higher MPRA activity than positive control sequences, albeit with far fewer tested elements[15]. Overall, these results suggest that TE-derived sequences possess the sequence potential for *cis*-regulatory activity as strong or stronger than their non-TE counterparts.

Next, we examined the frequency of variants found in the human population for TE-derived and non-TE cCREs based on the 1000 Genomes Project[45]. The expectation is that regions under functional constraint, like DNA elements regulating genes, would have fewer common variants, defined here as variants with human population allele frequency greater than 1%. Promoter distal TE-derived cCREs (dELS and CTCF-only) overlap variants less often than regions directly flanking them (Fig. 5B top, Supplementary Fig. 8). Furthermore, the frequency of common variants found in TE-derived cCREs is lower than their flanking regions apart from promoter sequences (PLS and DNase-H3K4me3) (Fig. 5B bottom, Supplementary Fig. 8). These results suggest that non-promoter TE-derived cCREs are under functional constraint and less tolerant of sequence variation than their surrounding sequences. However, TE-derived PLS, pELS, and dELS cCREs have significantly more common variants compared to non-TE cCREs, though the trend exists for all cCRE types. This indicates that TE-derived cCREs are generally less constrained in the human population than those apparently not derived from TEs.

Besides the epigenomic marks used by ENCODE to define cCREs, we used four additional metrics for identifying regulatory elements to compare the global profiles of TE-derived and non-TE cCREs: ATAC-seq for open chromatin, TF ChIP-seq for TF binding, MPRA for regulatory potential of the underlying sequence, and phastCons score for sequence conservation. As the vast majority of TE-derived cCREs are lineage-specific, we limited our analysis to TE-derived and non-TE cCREs that are found in human but not in mouse, allowing us to compare cCREs of roughly similar ages. Overall, TE-derived cCREs are not significantly different from non-TE cCREs in the proportion of elements that have any combination of ATAC-seq peaks, TF ChIP-seq peaks, MPRA activity, and high phastCons scores (Chi-square test, $p = 0.24$, Fig. 5C). This shows that the genomic features that are commonly used to annotate regulatory elements genome-wide are largely the same between TE and non-TE elements.

Finally, we investigated whether TE-derived cCREs could be physiologically relevant using the NHGRI-EBI GWAS catalog[46]. In addition

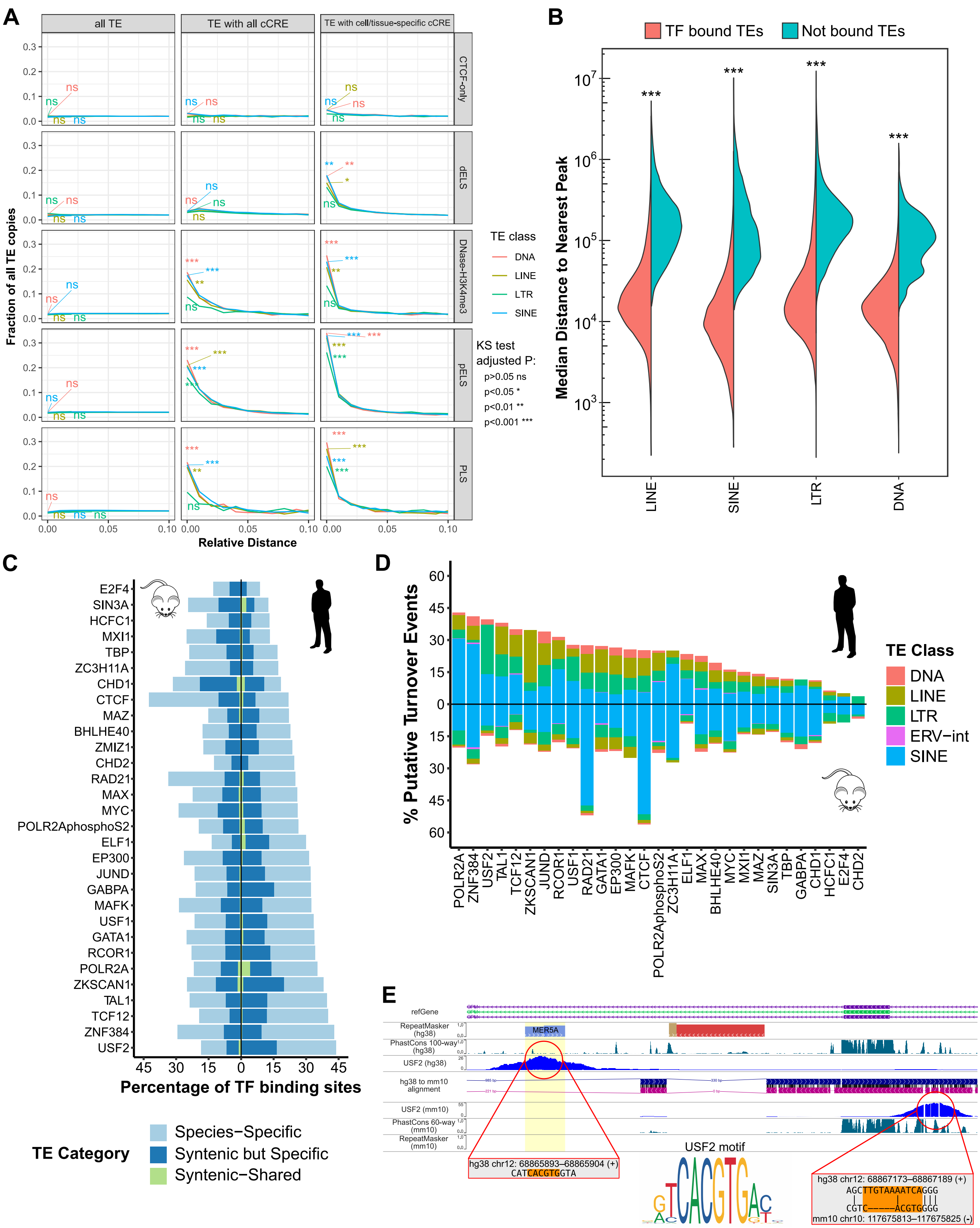

to the comprehensive list of top GWAS SNPs (GWAS variants), we divided SNPs into different parent terms as defined by EBI for physiologically related diseases and traits. Compared to randomly shuffled genomic coordinates, the general set of cCREs is enriched for GWAS variants across all GWAS parent terms, in line with a previous study (Fig. 5D, Supplementary Fig. 9)[47]. TE-derived cCREs are enriched for GWAS variants overall and in 11/17 parent terms (Supplementary Fig. 9, Supplementary Data 2). However, they have consistently lower enrichment for GWAS variants compared to non-TE cCREs, which may be due to underrepresented profiling of SNPs in TEs from genotyping arrays (Supplementary Data 2). Altogether, these results suggest that TE-derived cCREs are functionally comparable to non-TE cCREs and carry sequences that are physiologically important for human traits and disease.

Fig. 4 | Regulatory TEs cluster with non-TE regulatory elements and TEs provide TFBS turnover sites. A Relative distance of all TEs to cCREs, cCRE-associated TEs to all cCREs of the same type (cell agnostic), and cCRE-associated TEs to same cell/tissue type cCREs. Relative distances are further separated by TE class and cCRE type. See Supplementary Data 6 for KS test *p*-values. **B** Median distances for TF bound TEs (red) and non-bound TEs (blue) across 409 TFs in 535 TF ChIP-seq datasets. One-sided Wilcoxon rank-sum test was performed with Benjamini–Hochberg correction (p-value < 2.2×10^{-16} for all TE classes). **C** Percentage of TE-derived TFBSs for 30 TFs with ChIP-seq in human K562 and mouse MEL cells. TE percentage is further divided into binding sites that are species-specific with no synteny, binding sites that are species-specific with synteny, and binding sites that are shared. **D** Percentage of putative TFBS turnover events that come from TEs. Each percentage is split up by TE class contribution for the TF. **E** Browser shot of USF2 binding site turnover in human facilitated by primate lineage insertion of MER5A. Underlying USF2 motif sequence alignment in human and mouse are shown (if available). TF transcription factor, KS test Kolmogorov–Smirnov test. ***p < 0.001.

Discussion

TEs make up a large portion of most mammalian genomes, and many studies have shown that TEs contribute to their regulatory landscape. However, the extent to which TEs supply different types of regulatory elements and the factors that allow them to evolve as regulatory elements are not well understood. In this study, we utilize cCREs to define the contribution of TEs to the human regulatory space, finding that ~25% of all cCREs are TE-derived. This overall contribution is similar to previous estimates by Pehrsson et al. who studied the overlap of TEs with active regulatory states in the RoadMap Epigenome Project[22]. We observed that TEs do not contribute to the different types of cCREs equally; they contribute more substantially to gene-distal enhancers than to gene-proximal enhancers and promoters. This pattern is likely driven by selection against TE insertions in the proximity of genes[48]. Regardless of their cCRE type, we found that TE-derived cCREs are more likely to be restricted to one or a few cell/tissue types compared to non-TE cCREs. This result suggests that TEs could be important for regulatory innovation by providing gene regulatory elements that are active in a limited number of cellular contexts. The documented contribution of TEs to gene regulation in rapidly-evolving processes such as innate immunity and placentation support this hypothesis[13,49].

Different TEs have invaded and expanded in genomes at various points during evolution, leading to some being shared between species and others being lineage-specific. Andrews et al. had previously found that over 80% of primate-specific TFBS and cCREs overlap with TEs based on alignments of 241 mammalian genomes[50]. In contrast, we only identified ~29% of all human-lineage cCREs to be TE-derived based on cCRE annotations in human and mouse. The two main reasons for the difference in cCREs attributed to TEs are the definition of TE overlap and definition of primate-specific or human-lineage cCREs. First, Andrews et al. counted 1 bp intersection of cCRE and TE as overlap, whereas we were much more stringent in only counting a cCRE as overlapping if at least half of the cCRE sequence intersects with a single TE copy. Second, Andrews et al. looked only at primate-specific regions of the genome while we extended our analysis to include regions with synteny between human and mouse. By examining human-mouse shared cCREs, we found that TEs provide a small fraction (up to 2%) of conserved cCREs orthologous between human and mouse, though this may be an underestimation due to less extensive profiling of cells/tissues in mouse relative to human (839 and 157 cell/tissue types profiled in human and mouse, respectively). Thus, it is possible that we are underestimating the contribution of TEs to conserved regulatory elements and many TE-derived mouse cCREs have yet to be discovered. Including syntenic TEs in human and mouse also allowed us to gain additional insights. Among TEs that contribute to cCREs and are orthologous (shared by descent) between human and mouse, most are retained as or become cCREs in only one lineage, indicating either lineage-specific loss or lineage-specific gain of regulatory activity, respectively. Furthermore, a majority of non-orthologous, lineage-specific TE-cCREs come from TE subfamilies that are old enough to be found in both human and mouse (Supplementary Fig. 2). Taken together, our results suggest that most TE-derived regulatory elements come from old TEs. This is consistent with a previous study by Villar et al. which found that evolutionarily young enhancers were primarily adapted from ancestral DNA sequences over 100 million years of age[51].

To broadly understand where *cis*-regulatory activity in TEs comes from, we investigated the evolutionary origins of cCRE-associated TF motifs. In LINEs, LTR elements, and DNA transposons, cCRE-associated TF motifs originate from their consensus sequences more than expected by chance, suggesting an ancestral source for many important TE-derived TF motifs. As TEs age, the bulk of these TF motifs degrade over time. These results suggest that the amplification of these TEs disperses TF motifs available immediately upon insertion, but only a small subset is co-opted for host gene regulation. SINEs, which are extremely abundant in mammals (Alu elements alone account for 10% of the human genome sequence), show a very different trend compared to the other main TE classes. They have the lowest proportion of cCRE-associated TF motifs stemming from their consensus sequence, and the percentage of motifs that have an ancestral origin does not decrease as they age. Although SINEs have slightly higher substitution rates than L1s and DNA transposons of the same age, this does not explain the lack of relationship between TE subfamily age and percentage of cCRE-enriched TF motifs with ancestral origin[52]. These results suggest that SINEs provide relatively fewer mature TF motifs but instead frequently supply raw sequence material from which additional TF motifs emerge over time by mutation. This model is consistent with previous studies documenting the progressive birth of enhancers from Alu and RSINE1 elements in human and mouse, respectively[18,53]. Since SINEs have given rise to ~5% of human cCREs, these findings indicate that this “seed-and-mature” process has been a rich source of new *cis*-regulatory elements in the human genome.

When TEs insert themselves into the genome, the newly integrated copy and its progenitor are typically identical in sequence and therefore have the same sequence potential for *cis*-regulatory activity. However, only a small subset of TE copies within any given subfamily overlaps with cCREs. What influences some TE copies to retain or evolve *cis*-regulatory activity? One likely influential factor is the genomic context of the TE and its proximity to functional sequences such as genes and *cis*-regulatory elements[18]. Consistent with this model, we demonstrate that TEs with either cCREs or TFBSs have shorter genomic distance to non-TE cCREs or TFBSs compared to other TEs. Among TEs, the distance between LTR elements with cCREs/TFBSs and non-TE cCREs/TFBSs is the highest, indicating the relatively independent activity of LTRs, possibly due to high density of TFBSs in LTRs[54,55]. Based on the observation that TF bound TEs are close to non-TE TFBSs, we propose that the clustering of TFBSs from TE insertions introduces functional redundancy that can promote the turnover of TFBSs during evolution, as is prominent in mammals[39–42]. By examining the binding profiles of 30 TFs in human and mouse leukemia cell lines, we estimate that TEs have contributed 3–56% of all putative TFBS turnover events depending on the TF. Together these results suggest that the insertion of TEs near existing *cis*-regulatory elements is a major driver of TFBS evolutionary turnover.

An outstanding question for future studies is to determine the extent to which TE-derived cCREs have contributed to human adaptation and phenotypic variation. Our analysis brings hints that a

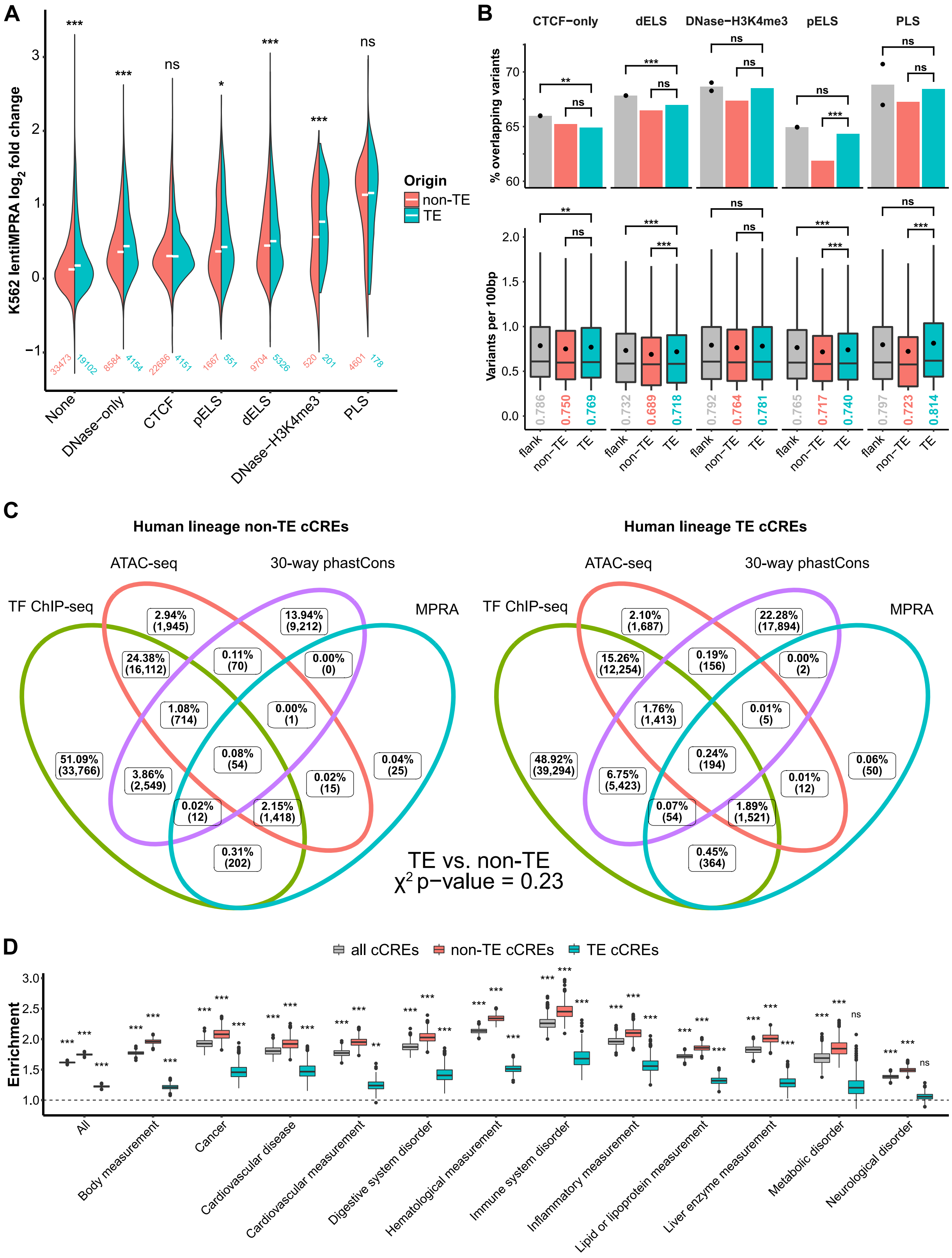

subset of TE-derived cCREs serve important biological functions. First, we found that the sequences of TE-derived cCREs are generally more evolutionarily constrained than their non-cCRE counterparts. Second, we observed that TE-derived cCREs are enriched for GWAS variants, albeit to a lesser extent than non-TE cCREs. While this could indicate that TEs are less likely to be physiologically relevant, it could also reflect technical shortcomings associated with genotyping within TE sequences. Genotyping arrays, which use short oligonucleotide probes to discern SNPs, are designed to avoid repetitive regions of the genome. Our analysis of nine genotyping arrays from Affymetrix and Illumina shows between 30 and 36% of SNPs located in repetitive DNA, short of the 45% TE content in the human genome (Supplementary Data 2). These observations suggest that GWAS studies may have missed trait-associated SNPs residing within TE

Fig. 5 | TE-derived cCREs share similar features with non-TE cCREs. A K562 lentiMPRA activity split by cCRE annotation or lack thereof. Number of TE and non-TE sequences tested for each group is listed. Median $\log_2$ fold change over negative control activity is displayed as a white dash. Two-sided Wilcoxon rank-sum test with Benjamini–Hochberg correction was performed to compare TE and non-TE sequence MPRA activity (None p-value = 4.13×10^{-91}, DNase-only p-value = 3.51×10^{-21}, CTCF p-value = 0.166, pELS p-value = 0.0223, dELS p-value = 7.19×10^{-10}, DNase-H3K4me3 p-value = 5.85×10^{-6}, PLS p-value = 0.195). **B** 1000 Genomes Project common variants (allele frequency >1%) in TE and non-TE cCREs. Percentage of cCREs that overlap common variants (top) and variants per 100 bp (bottom) are shown for each cCRE type. Percentages of common variant overlap for upstream and downstream cCRE flanking regions are shown as black dots (top). Mean variants per 100 bp is displayed by a black dot and listed below each boxplot (bottom). Outliers have been removed from boxplots. Comparisons between TE cCREs, non-TE cCREs, and flanking regions were done using permutation tests (1000 permutations, two-sided). The numbers of TE cCREs shown in the boxplot for CTCF-only, dELS, DNase-H3K4me3, pELS, and PLS cCREs are 14,110, 120,930, 5766, 14,787, and 1100. The numbers of non-TE cCREs shown in the boxplot for CTCF-only, dELS, DNase-H3K4me3, pELS, and PLS cCREs are 22,089, 305,405, 10,820, 63,862, and 16,508. The numbers of TE-cCRE flanking regions shown in the boxplot for CTCF-only, dELS, DNase-H3K4me3, pELS, and PLS cCREs are 28,609, 242,971, 11,514, 29,325, and 2185. See Supplementary Data 3 for p-values. **C** Venn diagram of human-lineage TE and non-TE cCRE overlap with TF ChIP-seq, ATAC-seq, 30-way phastCons, and MPRA activity. One-sided Chi-square test was performed to compare TE and non-TE cCRE overlaps. **D** Enrichment of GWAS variants by EBI EFO parent term for all cCREs, non-TE cCREs, and TE cCREs. Permutation test (1000 permutations, one-sided) was performed to compare observed overlap of cCREs with GWAS variants to shuffled genomic background. See Supplementary Data 2 for p-values. MPRA, massively parallel reporter assay; lentiMPRA, lentivirus-based MPRA. $^{**}p < 0.01$, $^{***}p < 0.001$, not significant (ns).

sequences and there is a need to consider TE-derived variants in follow-up studies to GWAS[56].

Here, we focused on K562 for analyses related to TF binding and turnover as well as MPRA functional assay support simply due to the abundance of data available in this cell line. However, it is important to note that K562 is a cancer cell line with many chromosomal abnormalities, including a near-triploid genome[57,58]. Changes in copy number may affect the results of epigenomic profiling assays, as previously demonstrated by the correlation between whole genome sequencing and POLR2A ChIP-seq[59]. There is also the possibility that some of the TE-cCREs in K562 are cancer-specific and shared across multiple cancer cell lines. We observed that K562 TE-cCREs are biased to being specific to K562, less shared across cancer cell lines than all cCREs, and depleted for promoter cCREs (Supplementary Fig. 1D, E). Since these trends in cancer cell lines are consistent with the overall trends for all TE-cCREs, it is likely that observations for TE-derived cCREs in K562 are generally applicable.

The nature of TEs as repetitive elements with rich and varied evolutionary histories raises challenges during their study. Mapping short reads back to TEs uniquely has been a long-standing problem. With the application of long, paired-end reads the problem has been largely alleviated, as demonstrated by Sexton and Han[60]. Therefore, the utilization of paired-end reads in ENCODE4 made it possible to reliably identify cCREs within most TEs. However, we still need to bear in mind that the cCREs within recent L1 subfamilies could still be undercounted in the study due to limitations in mapping. In addition, technical limitations in identifying particularly old TEs could have impacted several of our analyses. As TEs accumulate mutations over time, their sequences diverge from the consensus sequence used to annotate them. This can lead to incorrect or missing annotation, especially for RepeatMasker-based annotations which rely on alignment to consensus sequences[61,62]. In our human-mouse comparison, we observed that ~20% of TEs in syntenic regions were classified as belonging in the same repeat family but not assigned to the same subfamily. Although a few are real instances where different TEs created independent insertions in the same syntenic region, most cases likely arise due to a combination of high sequence divergence from the consensus sequence and high similarity between subfamily consensus sequences. Incorrect annotation of TE subfamily elements could have also affected our analyses that compare TE copies within their subfamily, like for cCRE-enriched TF motifs and their origins. Finally, since highly conserved regulatory elements are old by definition, TEs that provided the underlying regulatory element sequence may have already decayed past the point of recognition. Any missing TE annotations would have led to underestimating the scale of TE contribution to conserved regulatory elements, possibly including many gene-proximal or broadly used elements. It would be interesting to see if more sensitive TE detection methods would implicate TEs as significant contributors to regulatory elements of ancient origins.

In summary, we have shown that TEs are substantial contributors to *cis*-regulatory innovation and maintenance. We confirm previous reports that TEs make up ~25% of the human regulatory genome and provide direct, genome-wide functional evidence from K562 lentiMPRA. This is also reflected in the depletion of common human population variants and enrichment of GWAS variants in TE-derived cCREs relative to background. To gain insights into regulatory innovation, we quantify the proportion of lineage-specific regulatory elements in humans and mice that are derived from TEs (8–36% depending on type). By taking advantage of the phylogenetic relationship between TE copies in the same subfamily, we probe the origins of TF motifs for regulatory TEs, discovering that most TE classes bring TF motifs to be potentially co-opted while SINEs primarily gain regulatory TF motifs through mutations. Although most focus in the field has been on innovation, we demonstrate that TEs are active participants in maintaining regulatory features like TFBSs (3–56% of putative TF turnover events). Lastly, we provide evidence that TE genomic insertion site is potentially a general factor in determining which TE copies become regulatory elements. While many ideas are not completely novel to the field, this study has provided systematic analyses that explore whether the trends described in a handful of TE subfamilies are generally applicable. With TEs becoming increasingly recognized to be intertwined with how genomes have evolved and operate, we believe that our work will serve as an encyclopedia to help advance our understanding of fundamental biology and disease.

Methods

Annotation of TE-derived cCREs

Genomic cCRE annotations in hg38 (cell agnostic and 25 fully profiled ENCODE cell/tissue types) and mm10 were downloaded from (https://screen.wenglab.org/) and the ENCODE portal (https://www.encodeproject.org/)[19]. Genomic TE annotations in hg38 and mm10 were obtained from RepeatMasker (https://repeatmasker.org/)[63]. We used BedTools intersect[64] to find cCREs that are associated with TEs, requiring at least 50% of the cCRE to overlap a single TE.

Enrichment of TEs in cCREs

We calculated the enrichment of TE subfamilies for cCREs as follows.

$$\log_2 \frac{(\text{number of TE} - \text{cCRE elements})/(\text{total cCREs})}{(\text{total bp in TE subfamily})/(\text{genome size})} \tag{1}$$

For visualization, we included TE subfamilies with no overlap with cCREs as $\log_2$ enrichment of −10, which is lower than any subfamily with cCRE overlap.

Human-mouse cCRE comparison

To characterize human and mouse cCREs as shared or lineage-specific (Supplementary Fig. 2), we first used liftOver with -minMatch option of 0.1 to identify syntenic regions in the other species. The syntenic region was determined to be a cCRE or TE-derived if at least 50% of the syntenic region overlaps with a cCRE or TE. Syntenic regions with cCREs were classified as "shared" if the cCRE type was the same in both species and "different" if the cCRE type was different. TEs in syntenic regions of human and mouse were counted as orthologous if both TEs are annotated as belonging to the same TE family (e.g., SINE/Alu). To calculate the total number of human-specific cCREs, we started by summing syntenic human cCRE (394,610), non-syntenic human cCRE (167,134), and human TE-cCRE (215,752) categories from Fig. 2A. Then, we subtracted human TE-cCREs with a syntenic mouse cCRE but no syntenic TE (5361) and added orthologous TEs that are lineage-specific (15,973).

To compare sequence conservation, 100-way phastCons scores[65] were downloaded from https://genome.ucsc.edu/. Two-sided Wilcoxon rank-sum test was used for comparisons between groups of TE-cCREs.

Identification of cCRE-enriched TF motifs

First, TEs in each subfamily were separated based on overlap with hg38 cCREs, with subfamilies that lacked cCRE overlap removed from analysis ($n = 116$). Next, TE subfamilies were split into three groups depending on whether the length distributions of cCRE (foreground) and non-cCRE (background) elements were significantly different based on Kolmogorov–Smirnov (KS) test. One group of subfamilies ($n = 194$) have no significant difference with all background elements included. For the second group of subfamilies ($n = 993$) with significant difference in length distribution between foreground and background elements, background elements were binned and randomly selected to match the proportion of foreground elements found in each bin. Random selection of background elements in the second group of subfamilies was performed 10 times. TE subfamilies that could not achieve matched foreground/background length distributions were disregarded from further analysis ($n = 17$).

To identify cCRE-enriched motifs, we ran AME motif enrichment using the HOCOMOCOv11 human core transcription factor motif database[66] for each TE subfamily, with cCRE elements as foreground and non-cCRE elements (all elements or random selection) as background/control. Enriched motifs were grouped according to motif archetypes[47]. To confirm AME results, we scanned TE subfamily elements for the top enriched motif within each archetype and performed Fisher's exact test, further filtering for motifs that have significant association with cCRE annotation ($p < 0.05$ after multiple test correction with Benjamini–Hochberg method), at least 10 elements having both the motif and cCRE annotation, and odds ratios of at least 2. We also filtered for TF motifs that pass Fisher's exact test using TE subfamily consensus coverage-controlled background sequences, identifying TF motifs that distinguish cCRE overlapping TE copies from non-overlapping copies based on sequence variation alone.

Origin of cCRE-associated TF motifs

In order to estimate the percentage of cCRE-enriched motifs that were derived from an ancestral origin, we first derived consensus sequences for each TE subfamily from RepeatMasker and the RepBase-derived RepeatMasker Library 20170127 (Supplementary Methods). We could not obtain consensus sequences for four subfamilies (L2d, L2d2, Alu, and MLT1B-int), which were excluded from further analysis. Next, we scanned each consensus sequence for all HOCOMOCOv11 human core motifs. For each motif found in a TE subfamily's consensus sequence, we scanned all elements within the subfamily for the motif. The relative position of each motif to the consensus sequence was found by aligning each element to its consensus sequence using Needle pairwise alignment[67]. Finally, the percent ancestral origin rate of a given motif was calculated as the percentage of motifs that were within 10 bp of the consensus sequence motif. As we had grouped motifs based on motif archetype, we used the ancestral origin rate of the top enriched motif per archetype. In the case that the top motif was not found in the consensus sequence, we allowed for any other enriched motif in the archetype that was in the consensus to substitute. Any motif archetype that had no cCRE-enriched motif in the consensus sequence was assigned an ancestral origin rate of 0.

Relative distance of TE to closest cCRE

To estimate the spatial correlation between TEs and cCREs, we calculated relative distance first described by Favorov et al. and implemented within the BEDTools suite[64,68]. Briefly, for each cCRE type, TEs were assigned to their closest non-TE cCRE. Then, the distance between cCREs was split into 100 equal sized intervals and the frequency of TEs that fall within each interval was counted. We shuffled TE coordinates using bedtools shuffle 100 times to constitute the null hypothesis set, and applied KS test with Bonferroni multiple test correction to evaluate the difference between observation and shuffled null expectation.

Bound vs unbound TE distance to nearest TF peak

A total of 587 IDR thresholded TF ChIP-seq peak files in K562 were downloaded from ENCODE after filtering out those with "NOT_COMPLIANT" or "ERROR" audit labels. Supplementary Data 4 lists the TFs and ChIP-seq datasets that were used. For each TF, individual TEs were classified as bound if they intersected the peak summit and non-bound otherwise. We then calculated the linear distance from each TE to the nearest non-overlapping peak. For each TE subfamily with at least 10 TF bound individual TEs, we randomly sampled an equal number of non-bound individual TEs as those which were bound and ranked them in descending order of distance. After repeating random sampling 1000 times, we averaged each of the ranks across all 1000 samples to get a distribution of average distances to the nearest non-overlapping peak for non-bound TEs. We then calculated p-values using two-sided Wilcoxon rank-sum tests between bound and unbound TEs within each subfamily. We calculated the $\log_{10}$ ratio of average median distances to the nearest non-overlapping peak between bound and non-bound TEs as the following:

$$\log_{10}\frac{\text{Median distance to nearest non} - \text{TE peak (bound TEs)}}{\text{Median distance to nearestnon} - \text{TE peak (unbond TEs)}} \tag{2}$$

Identification of putative TF turnover events

IDR-thresholded peaks for 30 TF ChIP-seq datasets with matching K562 TF ChIP-seq were downloaded for mouse MEL from ENCODE[19]. Syntenic regions to TF binding peaks were identified with the same method described above for human-mouse comparison. If a TF peak in one species overlapped at least 50% of a peak in the other species, it was classified as "shared". Otherwise, the TF peak was classified as "syntenic but specific" for alignable sequences but with species-specific TF binding. To identify putative TFBS turnover events after human-mouse divergence, we identified all TF peaks in one species within 5 kb of the syntenic region of a TF peak in the other species (Supplementary Fig. 7A). For each peak, mean phastCons score was assigned using 100-way vertebrate phastCons scores in human or 60-way vertebrate phastCons scores in mouse[65]. We calculated the median phastCons score for conserved TF binding peaks in human and mouse to infer human-mouse ancestral TF binding. For each pair of lineage-specific peaks, the human-mouse ancestral TFBS was inferred based on human-mouse synteny and phastCons score higher than the median phastCons score for conserved TF binding peaks. Pairs of lineage-specific peaks were identified as putative TFBS turnover events if a single non-ancestral TF binding peak was within 5 kb of an ancestral TF binding peak. TE-derived peaks were classified using the prior mentioned criteria of 50% overlap with the TF binding peak.

MPRA comparison

K562 lentiMPRA data was downloaded from the ENCODE portal[44]. TE-derived or non-TE-derived cCRE annotations were intersected with lentiMPRA sequence coordinates and then assigned the maximum $\log_2$ fold change (log2FC) value (both strands). cCREs were grouped based on their annotation with the following exceptions: "None" = Low-DNase or no intersection, "CTCF" = any classification bound by CTCF. Two-sided Wilcoxon rank-sum test was performed comparing the log2FC values of TE-derived cCREs with non-TE-derived cCREs within the same category. An alternative hypothesis of TE-derived cCREs having a greater log2FC value than non-TE-derived cCREs was used. *P*-values for all tests underwent Benjamini–Hochberg multiple-test correction.

Human population variant frequency in cCREs

We extracted variants within the human population characterized by the 1000 genomes project[45] and further selected variants with allele frequency >1% as common variants. For each cCRE that did not overlap coding sequence in GENCODEv41[69], we counted how many common variants intersect with them, and the number of common variants was normalized per 100 bp of sequence. The percentage with variant overlap and the distribution of variants per 100 bp was obtained for TE-derived cCREs, non-TE cCREs, and cCRE flanking regions. Flanking regions were defined as non-coding genomic regions directly upstream and downstream with the same length as the cCRE. Permutation tests were then performed to compare percentage with variant overlap and mean variants per 100 bp between TE-derived cCREs, non-TE cCREs, and cCRE flanking regions relative to random genomic background (Supplementary Data 3, Supplementary Methods).

Venn Diagram comparing features for TE-derived and non-TE-derived cCREs

ATAC-seq in K562 cells were downloaded from ENCODE and 30-way (27 primates) phastCons scores were downloaded from https://genome.ucsc.edu/. Non-TE and TE-derived cCREs were classified as being accessible (ATAC-seq), bound by a TF (TF ChIP-seq), MPRA active (MPRA), or having high levels of sequence conservation among primates (phastCons). PhastCons scores were binned into 20 bp windows and each cCRE was assigned the mean of intersecting phastCons scores. cCREs with the top 10% of phastCons scores were selected as high sequence conservation. For ATAC-seq and TF ChIP-seq, a cCRE containing a peak summit within its interval was considered accessible or bound, respectively. MPRA log2FC was obtained for each cCRE as previously described, and cCREs were classified as active in MPRA if the maximum log2FC was greater than 1. Finally, a Venn Diagram was generated using the combined classification of cCREs. Chi-square test was performed to test for differences in feature classification between TE- and non-TE-derived cCREs.

Enrichment of cCREs in GWAS variants

The NHGRI-EBI GWAS catalog with added ontology annotations and GWAS to EFO mappings was downloaded from http://www.ebi.ac.uk/gwas[46]. The strongest SNP was chosen for each reported entry. We used dbSNP153[70] to assign chromosome positions in hg38 to SNPs if chromosome position was not already listed; SNPs with neither chromosome position nor dbSNP153 rs ID were excluded. The number of GWAS SNPs found in cCREs was counted following BEDTools overlap[64]. Each SNP was counted at most once for each parent term. Permutation test by genome-wide shuffling of cCRE coordinates was performed 1000 times to obtain a random expectation for GWAS SNP overlap. Enrichment was calculated as the number of overlapping GWAS variants in cCREs divided by the number of overlapping GWAS variants in random shuffled coordinates. *P*-value was defined as the proportion of random shuffles that reached the number of overlapping GWAS variants in cCREs or higher. As a negative control, we shuffled cCRE coordinates an additional 100 times and took the mean number of GWAS variant overlaps.

Statistics and reproducibility

No statistical method was used to predetermine sample size (all TEs and datasets were used where reasonable). All data points were included in statistical analysis. Statistical analyses and graphical representations were performed using R versions 3.5.1 and 4.0.1.

Reporting summary

Further information on research design is available in the Nature Portfolio Reporting Summary linked to this article.

Data availability

All accession codes and download links for publicly available data are listed in Supplementary Data 1. Source data are provided with this paper.

Code availability

All code for analysis is available at https://github.com/twlab/ENCODE_TE[71].

References

1. McClintock, B. The origin and behavior of mutable loci in maize. *Proc. Natl Acad. Sci. USA* **36**, 344 (1950).
2. Osmanski, A. B. et al. Insights into mammalian TE diversity through the curation of 248 genome assemblies. *Science* **380**, eabn1430 (2023).
3. Nurk, S. et al. The complete sequence of a human genome. *Science* **376**, 44–53 (2022).
4. Wells, J. N. & Feschotte, C. A field guide to eukaryotic transposable elements. *Annu. Rev. Genet.* **54**, 539–561 (2020).
5. Christmas, M. J. et al. Evolutionary constraint and innovation across hundreds of placental mammals. *Science* **380**, eabn3943 (2023).
6. Rebollo, R., Romanish, M. T. & Mager, D. L. Transposable elements: an abundant and natural source of regulatory sequences for host genes. *Annu. Rev. Genet.* **46**, 21–42 (2012).
7. Chuong, E. B., Elde, N. C. & Feschotte, C. Regulatory activities of transposable elements: from conflicts to benefits. *Nat. Rev. Genet.* **18**, 71–86 (2017).
8. Bourque, G. et al. Ten things you should know about transposable elements. *Genome Biol.* **19**, 199 (2018).
9. Sundaram, V. & Wysocka, J. Transposable elements as a potent source of diverse cis-regulatory sequences in mammalian genomes. *Philos. Trans. R. Soc. B* **375**, 20190347 (2020).
10. Fueyo, R., Judd, J., Feschotte, C. & Wysocka, J. Roles of transposable elements in the regulation of mammalian transcription. *Nat. Rev. Mol. Cell Biol.* **23**, 481–497 (2022).
11. Lawson, H. A., Liang, Y. & Wang, T. Transposable elements in mammalian chromatin organization. *Nat. Rev. Genet.* https://doi.org/10.1038/s41576-023-00609-6 (2023).
12. Wang, T. et al. Species-specific endogenous retroviruses shape the transcriptional network of the human tumor suppressor protein p53. *Proc. Natl Acad. Sci. USA* **104**, 18613–18618 (2007).
13. Chuong, E. B., Elde, N. C. & Feschotte, C. Regulatory evolution of innate immunity through co-option of endogenous retroviruses. *Science* **351**, 1083–1087 (2016).
14. Sundaram, V. et al. Functional cis-regulatory modules encoded by mouse-specific endogenous retrovirus. *Nat. Commun.* **8**, 14550 (2017).

15. Du, A. Y. et al. Functional characterization of enhancer activity during a long terminal repeat's evolution. *Genome Res* **32**, 1840–1851 (2022).
16. Zemojtel, T., Kielbasa, S. M., Arndt, P. F., Chung, H. R. & Vingron, M. Methylation and deamination of CpGs generate p53-binding sites on a genomic scale. *Trends Genet.* **25**, 63–66 (2009).
17. Zemojtel, T. et al. CpG deamination creates transcription factor–binding sites with high efficiency. *Genome Biol. Evol.* **3**, 1304–1311 (2011).
18. Judd, J., Sanderson, H. & Feschotte, C. Evolution of mouse circadian enhancers from transposable elements. *Genome Biol.* **22**, 1–26 (2021).
19. The ENCODE Project Consortium. et al. Expanded encyclopaedias of DNA elements in the human and mouse genomes. *Nature* **583**, 699–710 (2020).
20. Roadmap Epigenomics Consortium. et al. Integrative analysis of 111 reference human epigenomes. *Nature* **518**, 317–330 (2015).
21. Trizzino, M., Kapusta, A. & Brown, C. D. Transposable elements generate regulatory novelty in a tissue-specific fashion. *BMC Genomics* **19**, 468 (2018).
22. Pehrsson, E. C., Choudhary, M. N. K., Sundaram, V. & Wang, T. The epigenomic landscape of transposable elements across normal human development and anatomy. *Nat. Commun.* **10**, 1–16 (2019).
23. Brocks, D. et al. DNMT and HDAC inhibitors induce cryptic transcription start sites encoded in long terminal repeats. *Nat. Genet.* **49**, 1052–1060 (2017).
24. Schmidt, D. et al. Waves of retrotransposon expansion remodel genome organization and CTCF binding in multiple mammalian lineages. *Cell* **148**, 335–348 (2012).
25. Choudhary, M. N. K. et al. Co-opted transposons help perpetuate conserved higher-order chromosomal structures. *Genome Biol.* **21**, 1–14 (2020).
26. Choudhary, M. N. K., Quaid, K., Xing, X., Schmidt, H. & Wang, T. Widespread contribution of transposable elements to the rewiring of mammalian 3D genomes. *Nat. Commun.* **14**, 1–12 (2023).
27. Simonti, C. N., Pavličev, M. & Capra, J. A. Transposable element exaptation into regulatory regions is rare, influenced by evolutionary age, and subject to pleiotropic constraints. *Mol. Biol. Evol.* **34**, 2856 (2017).
28. Diehl, A. G., Ouyang, N. & Boyle, A. P. Transposable elements contribute to cell and species-specific chromatin looping and gene regulation in mammalian genomes. *Nat. Commun.* **11**, 1–18 (2020).
29. Kuhn, R. M., Haussler, D. & James Kent, W. The UCSC genome browser and associated tools. *Brief. Bioinform.* **14**, 144–161 (2013).
30. Chinwalla, A. T. et al. Initial sequencing and comparative analysis of the mouse genome. *Nature* **420**, 520–562 (2002).
31. Jordan, I. K., Rogozin, I. B., Glazko, G. V. & Koonin, E. V. Origin of a substantial fraction of human regulatory sequences from transposable elements. *Trends Genet.* **19**, 68–72 (2003).
32. Van De Lagemaat, L. N., Landry, J. R., Mager, D. L. & Medstrand, P. Transposable elements in mammals promote regulatory variation and diversification of genes with specialized functions. *Trends Genet.* **19**, 530–536 (2003).
33. Lowe, C. B., Bejerano, G. & Haussler, D. Thousands of human mobile element fragments undergo strong purifying selection near developmental genes. *Proc. Natl Acad. Sci. USA* **104**, 8005–8010 (2007).
34. Feschotte, C. Transposable elements and the evolution of regulatory networks. *Nat. Rev. Genet.* **9**, 397–405 (2008).
35. Swergold, G. D. Identification, characterization, and cell specificity of a human LINE-1 promoter. *Mol. Cell. Biol.* **10**, 6718–6729 (1990).
36. Minakami, R. et al. Identification of an internal cis-element essential for the human Li transcription and a nuclear factor(s) binding to the element. *Nucleic Acids Res.* **20**, 3139–3145 (1992).
37. Alexandrova, E. A. et al. Sense transcripts originated from an internal part of the human retrotransposon LINE-1 5′ UTR. *Gene* **511**, 46–53 (2012).
38. Sun, X. et al. Transcription factor profiling reveals molecular choreography and key regulators of human retrotransposon expression. *Proc. Natl. Acad. Sci. USA*. https://doi.org/10.1073/pnas.1722565115 (2018).
39. Stefflova, K. et al. Cooperativity and rapid evolution of cobound transcription factors in closely related mammals. *Cell* **154**, 530–540 (2013).
40. Yue, F. et al. A comparative encyclopedia of DNA elements in the mouse genome. *Nature* **515**, 355–364 (2014).
41. Cheng, Y. et al. Principles of regulatory information conservation between mouse and human. *Nature* **515**, 371–375 (2014).
42. Vierstra, J. et al. Mouse regulatory DNA landscapes reveal global principles of cis-regulatory evolution. *Science* **346**, 1007–1012 (2014).
43. Sundaram, V. et al. Widespread contribution of transposable elements to the innovation of gene regulatory networks. *Genome Res.* **24**, 1963–1976 (2014).
44. Agarwal, V. et al. Massively parallel characterization of transcriptional regulatory elements in three diverse human cell types. Preprint at *bioRxiv* https://doi.org/10.1101/2023.03.05.531189 (2023).
45. The 1000 Genomes Project Consortium. A global reference for human genetic variation. *Nature* **526**, 68–74 (2015).
46. Sollis, E. et al. The NHGRI-EBI GWAS Catalog: knowledgebase and deposition resource. *Nucleic Acids Res.* **51**, D977–D985 (2023).
47. Vierstra, J. et al. Global reference mapping of human transcription factor footprints. *Nature* **583**, 729–736 (2020).
48. Medstrand, P., Van De Lagemaat, L. N. & Mager, D. L. Retroelement distributions in the human genome: variations associated with age and proximity to genes. *Genome Res.* **12**, 1483–1495 (2002).
49. Lynch, V. J., Leclerc, R. D., May, G. & Wagner, G. P. Transposon-mediated rewiring of gene regulatory networks contributed to the evolution of pregnancy in mammals. *Nat. Genet.* **43**, 1154–1159 (2011).
50. Andrews, G. et al. Mammalian evolution of human cis-regulatory elements and transcription factor binding sites. *Science* **380**, eabn7930 (2023).
51. Villar, D. et al. Enhancer evolution across 20 mammalian species. *Cell* **160**, 554–566 (2015).
52. Pace, J. K. & Feschotte, C. The evolutionary history of human DNA transposons: evidence for intense activity in the primate lineage. *Genome Res.* **17**, 422–432 (2007).
53. Su, M., Han, D., Boyd-Kirkup, J., Yu, X. & Han, J. D. J. Evolution of Alu elements toward enhancers. *Cell Rep.* **7**, 376–385 (2014).
54. Thompson, P. J., Macfarlan, T. S. & Lorincz, M. C. Long terminal repeats: from parasitic elements to building blocks of the transcriptional regulatory repertoire. *Mol. Cell* **62**, 766–776 (2016).
55. Ito, J. et al. Systematic identification and characterization of regulatory elements derived from human endogenous retroviruses. *PLOS Genet* **13**, e1006883 (2017).
56. Payer, L. M. et al. Structural variants caused by Alu insertions are associated with risks for many human diseases. *Proc. Natl Acad. Sci. USA* **114**, E3984–E3992 (2017).
57. Gribble, S. M. et al. Cytogenetics of the chronic myeloid leukemia-derived cell line K562: karyotype clarification by multicolor fluorescence in situ hybridization, comparative genomic hybridization, and locus-specific fluorescence in situ hybridization. *Cancer Genet. Cytogenet.* **118**, 1–8 (2000).
58. Naumann, S., Reutzel, D., Speicher, M. & Decker, H. J. Complete karyotype characterization of the K562 cell line by combined application of G-banding, multiplex-fluorescence in situ hybridization, fluorescence in situ hybridization, and comparative genomic hybridization. *Leuk. Res.* **25**, 313–322 (2001).

59. Zhou, B. et al. Comprehensive, integrated, and phased whole-genome analysis of the primary ENCODE cell line K562. *Genome Res.* **29**, 472–484 (2019).
60. Sexton, C. E. & Han, M. V. Paired-end mappability of transposable elements in the human genome. *Mob. DNA* **10**, 1–11 (2019).
61. de Koning, A. P. J., Gu, W., Castoe, T. A., Batzer, M. A. & Pollock, D. D. Repetitive elements may comprise over two-thirds of the human genome. *PLOS Genet.* **7**, e1002384 (2011).
62. Matsushima, W., Planet, E. & Trono, D. Ancestral genome reconstruction enhances transposable element annotation by identifying degenerate integrants. *Cell Genomics* **4**, 100497 (2024).
63. Smit, A., Hubley, R. & Green, P. RepeatMasker Open-4.0. 2013–2015 http://www.repeatmasker.org (2015).
64. Quinlan, A. R. & Hall, I. M. BEDTools: a flexible suite of utilities for comparing genomic features. *Bioinformatics* **26**, 841–842 (2010).
65. Siepel, A. et al. Evolutionarily conserved elements in vertebrate, insect, worm, and yeast genomes. *Genome Res.* **15**, 1034–1050 (2005).
66. Kulakovskiy, I. V. et al. HOCOMOCO: towards a complete collection of transcription factor binding models for human and mouse via large-scale ChIP-Seq analysis. *Nucleic Acids Res.* **46**, D252–D259 (2018).
67. Needleman, S. B. & Wunsch, C. D. A general method applicable to the search for similarities in the amino acid sequence of two proteins. *J. Mol. Biol.* **48**, 443–453 (1970).
68. Favorov, A. et al. Exploring massive, genome scale datasets with the GenometriCorr package. *PLOS Comput. Biol.* **8**, e1002529 (2012).
69. Frankish, A. et al. GENCODE 2021. *Nucleic Acids Res.* **49**, D916–D923 (2021).
70. Sherry, S. T., Ward, M. & Sirotkin, K. dbSNP—database for single nucleotide polymorphisms and other classes of minor genetic variation. *Genome Res.* **9**, 677–679 (1999).
71. Du, A. Y., Chobirko, J. D., Zhuo, X., Feschotte, C. & Wang, T. Regulatory transposable elements in the encyclopedia of DNA elements. twlab/ENCODE_TE. https://doi.org/10.5281/zenodo.12822146 (2024).

Acknowledgements

This work was supported by NIH grants R01HG007175 and U01HG009391. A.Y.D. was supported by NHGRI training grant T32HG000045. J.D.C. was supported by NIGMS MIRA (2R35GM122550-06).

Author contributions

T.W. and C.F. conceived the project. A.Y.D., J.D.C., and X.Z. designed and performed analysis. All authors took part in writing the manuscript.

Competing interests

The authors declare no competing interests.

Additional information

Supplementary information The online version contains supplementary material available at https://doi.org/10.1038/s41467-024-51921-6.

Correspondence and requests for materials should be addressed to Cédric Feschotte or Ting Wang.

Peer review information *Nature Communications* thanks the anonymous reviewers for their contribution to the peer review of this work. A peer review file is available.

Reprints and permissions information is available at http://www.nature.com/reprints

Publisher's note Springer Nature remains neutral with regard to jurisdictional claims in published maps and institutional affiliations.